Author's interactive comments

Dears referees, editors.

Thanks for your attentive manuscript analysis and for the comments to the manuscript. I agree with your comments and basing on these comments, I have selected several important partitions that additionally require better description and discussion here.

Boundary conditions

Eq (4) are the three momentum equations that differ from the initial momentum equations (1) so that they include the standard (typical) well-known boundary conditions (3). The procedure of this inclusion consists of the following successive steps.

1) We rewrite, for instance, the first equation using new variables:

$$\frac{\partial \sigma_{xx}}{\partial x} + \eta'_x \frac{\partial \sigma_{xx}}{\partial \eta} + \xi'_x \frac{\partial \sigma_{xx}}{\partial \xi} + \eta'_y \frac{\partial \sigma_{xy}}{\partial \eta} + \xi'_y \frac{\partial \sigma_{xy}}{\partial \xi} + \xi'_z \frac{\partial \sigma_{xz}}{\partial \xi} = \rho \frac{\partial^2 U}{\partial t^2};$$

2) We write the approximation of the derivative $\frac{\partial \sigma_{xz}}{\partial \xi}$ at the ice-shelf base towards the substance (glacier):

$$\left(\xi'_z \frac{\partial \sigma_{xz}}{\partial \xi}\right)^{N_\xi} = -\frac{1}{H}\left(\frac{\partial \sigma_{xz}}{\partial \xi}\right)^{N_\xi} \approx -\frac{1}{H}\frac{1}{2\,\Delta\xi}\sigma_{xz}^{N_\xi-2} + \frac{1}{H}\frac{4}{2\,\Delta\xi}\sigma_{xz}^{N_\xi-1} - \frac{1}{H}\frac{3}{2\,\Delta\xi}\sigma_{xz}^{N_\xi};$$

3) The standard (typical) boundary conditions at the ice - shelf base (3) requires that $\sigma_{xz} = \sigma_{xx}\frac{\partial h_b}{\partial x} + \sigma_{xy}\frac{\partial h_b}{\partial y} + P\frac{\partial h_b}{\partial x}$. Thus, we should replace the $\sigma_{xz}^{N_\xi}$ in agreement with the standard boundary conditions, with $\left\{\sigma_{xx}\frac{\partial h_b}{\partial x} + \sigma_{xy}\frac{\partial h_b}{\partial y}\right\}^{N_\xi} + P\frac{\partial h_b}{\partial x}$. Finally, we obtain the following approximation of the derivative $\left(\xi'_z \frac{\partial \sigma_{xz}}{\partial \xi}\right)^{N_\xi}$ at the ice-shelf base:

$$\left(\xi'_z \frac{\partial \sigma_{xz}}{\partial \xi}\right)^{N_\xi} \approx -\frac{1}{H}\frac{1}{2\,\Delta\xi}\sigma_{xz}^{N_\xi-2} + \frac{1}{H}\frac{4}{2\,\Delta\xi}\sigma_{xz}^{N_\xi-1} - \frac{1}{H}\frac{3}{2\,\Delta\xi}\left\{\sigma_{xx}\frac{\partial h_b}{\partial x} + \sigma_{xy}\frac{\partial h_b}{\partial y}\right\}^{N_\xi} - \frac{1}{H}\frac{3}{2\,\Delta\xi}P'\frac{\partial h_b}{\partial x} - \frac{3}{2\,\Delta\xi}\rho g\frac{\partial h_b}{\partial x};$$

$$P = \rho g H + P';$$

4) Thus, at the ice shelf base, we apply the equation

$$\left(\frac{\partial \sigma_{xx}}{\partial x}\right)^{N_\xi} + \left(\eta'_x \frac{\partial \sigma_{xx}}{\partial \eta}\right)^{N_\xi} + \left(\xi'_x \frac{\partial \sigma_{xx}}{\partial \xi}\right)^{N_\xi} + \left(\eta'_y \frac{\partial \sigma_{xy}}{\partial \eta}\right)^{N_\xi} + \left(\xi'_y \frac{\partial \sigma_{xy}}{\partial \xi}\right)^{N_\xi} - \frac{1}{H}\frac{1}{2\,\Delta\xi}\sigma_{xz}^{N_\xi - 2} +$$
$$+ \frac{1}{H}\frac{4}{2\,\Delta\xi}\sigma_{xz}^{N_\xi - 1} - \frac{1}{H}\frac{3}{2\,\Delta\xi}\left\{\sigma_{xx}\frac{\partial h_b}{\partial x} + \sigma_{xy}\frac{\partial h_b}{\partial y}\right\}^{N_\xi} - \frac{1}{H}\frac{3}{2\,\Delta\xi}P'\frac{\partial h_b}{\partial x} \approx \frac{3}{2\,\Delta\xi}\rho g\frac{\partial h_b}{\partial x} + \rho\left(\frac{\partial^2 U}{\partial t^2}\right)^{N_\xi},$$

which is the first equation from Eq (4), instead of the standard equation $\sigma_{xz} = \sigma_{xx}\frac{\partial h_b}{\partial x} + \sigma_{xy}\frac{\partial h_b}{\partial y} + P\frac{\partial h_b}{\partial x}$.

The same algorithm leads us to the similar equations on ice-shelf surface, ice-shelf front/terminus, ice-shelf lateral edges. For instance, at ice-shelf terminus these equations are expressed as

$$\begin{cases} \frac{1}{2\,\Delta x}\sigma_{xx}^{N_x-2} - \frac{4}{2\,\Delta x}\sigma_{xx}^{N_x-1} \approx -\frac{3}{2\,\Delta x}f(\xi) - \left(\xi'_x\right)^{N_x}\frac{\partial f(\xi)}{\partial \xi} + \rho\left(\frac{\partial^2 U}{\partial t^2}\right)^{N_x}; \\ \frac{1}{2\,\Delta x}\sigma_{yx}^{N_x-2} - \frac{4}{2\,\Delta \xi}\sigma_{yx}^{N_x-1} + \left(\frac{\partial \sigma_{yx}}{\partial x}\right)^{N_\xi} + \left(\eta'_y \frac{\partial \sigma_{yy}}{\partial \eta}\right)^{N_x} + \left(\xi'_y \frac{\partial \sigma_{yy}}{\partial \xi}\right)^{N_x} + \left(\xi'_z \frac{\partial \sigma_{zz}}{\partial \xi}\right)^{N_x} \\ \qquad \approx \rho\left(\frac{\partial^2 V}{\partial t^2}\right)^{N_x}; \\ \frac{1}{2\,\Delta x}\sigma_{yx}^{N_x-2} - \frac{4}{2\,\Delta \xi}\sigma_{yx}^{N_x-1} + + \left(\eta'_y \frac{\partial \sigma_{zy}}{\partial \eta}\right)^{N_x} + \left(\xi'_y \frac{\partial \sigma_{zy}}{\partial \xi}\right)^{N_x} + \left(\xi'_z \frac{\partial \sigma_{zz}}{\partial \xi}\right)^{N_x} \\ \qquad \approx \rho g + \rho\left(\frac{\partial^2 W}{\partial t^2}\right)^{N_x}; \end{cases} \quad (1A)$$

Where $f(\xi) = \begin{cases} 0, & \xi < \frac{h_s}{H}; \\ \rho_w g\,(h_s - \xi H), & \xi \geq \frac{h_s}{H}. \end{cases}$

If we withdraw Eq (4) from the mathematical formulation, then a reader will suppose that the modelling, in effect, can be performed with standard boundary conditions. However, the numerical experiments with the standard boundary conditions were not successful in the full model, which includes the momentum equations for the ice shelf as well as the wave equation for the sub-ice-shelf water. Thus, an additional suitable method should be suggested in the full model based on the coupling of the momentum equations with the wave equation.

Furthermore, in (Konovalov, 2012, 2014) I considered the first-order numerical approximations in the boundary conditions with intent to minimize the routine that is required to perform these approximations. While in this manuscript I employ the second-order numerical approximations that enhances the routine, but improves the implementation of the model.

Of course, a new approach/method requires confirmation by the experimental data and validation by the comparison with the results obtained by other models. While a measurement in the conditions of the resonant impact is the challenge, the models comparison (quantitative comparison) can be easily carried out.

Comparison of results obtained by the full model and by the Holdsworth & Glynn model

In the numerical experiments carried out for comparison of the two models I considered the forced vibration problem, which is described in the manuscript. For convenience and to avoid possible uncertainties in the interpretation of the forced vibrations modelled by the Houldsworth & Glynn model, I write here the full mathematical formulation of the Houldsworth & Glynn forced vibration model, which I considered in the test experiments. Here, I have kept notation, which is used in (Houldsworth & Glynn, 1978), except for the vertical deflection $W(x, y, t)$.

Thin-plate vibration equation (the momentum equation) is

$$\frac{\partial^2 M_x}{\partial x^2} + \frac{\partial^2 M_y}{\partial y^2} - 2\,\frac{\partial^2 M_{xy}}{\partial x\,\partial y} = \rho\, h\,\frac{\partial^2 W}{\partial t^2} + \rho_w g\, W - P';$$

where $M_x = -D\left(\frac{\partial^2 W}{\partial x^2} + \nu\,\frac{\partial^2 W}{\partial y^2}\right)$; $M_y = -D\left(\frac{\partial^2 W}{\partial y^2} + \nu\,\frac{\partial^2 W}{\partial x^2}\right)$; $M_{xy} = D(1-\nu)\,\frac{\partial^2 W}{\partial x\,\partial y}$;

$D = \frac{E\,h^3}{12\,(1-\nu^2)}$.

The wave equation for water layer is

$$\frac{\partial^2 W}{\partial\, t^2} = \frac{1}{\rho_w}\frac{\partial}{\partial\, x}\left(d_0\frac{\partial\, P\prime}{\partial\, x}\right) + \frac{1}{\rho_w}\frac{\partial}{\partial\, y}\left(d_0\frac{\partial\, P\prime}{\partial\, y}\right);$$

where P' is the deviation from the hydrostatic pressure.

The boundary conditions are

a) At $x = 0$ (fixed boundary): $W = 0$; $\frac{\partial W}{\partial x} = 0$; $M_x = \frac{1}{\nu}M_y$; $M_{xy} = 0$; $\frac{\partial P\prime}{\partial x} = 0$.

b) At $x = L_x$ (ice-shelf terminus): $M_x = 0$; $M_y = D\,\frac{1-\nu^2}{\nu}\,\frac{\partial^2 W}{\partial x^2}$; $\frac{\partial\, M_x}{\partial x} = 2\,\frac{\partial\, M_{xy}}{\partial y}$; $M_{xy} = D\,(1-\nu)\,\frac{\partial^2 W}{\partial x\,\partial y}$; $P' = A\rho_w g \sin\omega t$; where A is the amplitude of the incident wave, ω is the frequency of the forcing (incident wave).

c) At $x = 0$, $x = L_y$ (lateral edges of the ice-shelf): $M_y = 0$; $M_x = D\,\frac{1-\nu^2}{\nu}\,\frac{\partial^2 W}{\partial y^2}$; $\frac{\partial\, M_y}{\partial y} = 2\,\frac{\partial\, M_{xy}}{\partial x}$; $M_{xy} = D\,(1-\nu)\,\frac{\partial^2 W}{\partial x\,\partial y}$; $\frac{\partial\, P\prime}{\partial y} = 0$.

Additionally to the ice-shelf geometry considered in the manuscript, I have carried out three experiments with different geometries of the ice-shelf. Relying on your comments, I consider these experiments likewise as a comparative modelling, which is suggested for quantitative comparison of the two models discussed here. Figure 1A shows the geometries of the ice shelf in these three experiments respectively.

In the experiment A ice-shelf thickness and the water layer depth are constant values (Fig. 1A, a), while in the experiment B the expanding water layer is considered (Fig. 1A, b). A difference in the spectrums obtained in these two experiments, implies the impact of the cavity geometry to the eigen-frequencies of the shelf-water system. In the experiment C the tapering ice-shelf is considered (Fig. 1A, c).

Figures 2A..4A show the amplitude spectrums obtained in these three experiments respectively. The amplitude spectrums in Fig. 2A and in Fig. 4A are split up into parts for better visualization of the resonant peaks in the spectrums.

Figures 5A..7A show the ice-shelf deflections that respond to the eigen-frequencies derived from the amplitude spectrums in the Experiment A and in the Experiment C.

Figure 8A shows the shear stress distributions in the vertical cross-section along the centre-line.

Experiment A. The first three eigenvalues can be distinguished easily in the spectrums in Fig. 2A. They are approximately equal to 34.6s, 13.3s, 6.7s in the full model and are approximately equal to 42s, 14.2s, 6.8s, respectively, in the Holdsworth and Glynn model. The maximum difference between the eigenvalues is observed for the first eigenvalue, which corresponds to the largest peak in the spectrums in Fig. 2A. The relative deviation for the first eigenvalue is approximately equal to 20%. Then, we observe that the difference between the eigenvalues successively diminishes, so that the third resonant peaks in the full model almost align with the third peak in the Holdsworth and Glynn model. Nevertheless, further insight into the spectrum reveals a small increase of the deviation again (Fig. 2A, b). Moreover, the fourth eigenvalue (periodicity) becomes higher in the full model (Fig. 2A, b). Hence, in effect, the spacing in the full model between the first four resonant peaks is smaller than in the Holdsworth and Glynn model. The deflections obtained by the two models, are in agreement in the spatial distributions of nodes/antinodes for the first three modes (Fig. 5A).

Experiment B reveals the same trend in the difference between the eigenvalues obtained from the both considered models (Fig. 3A). I mean the successive diminishing of the deviation like in the preceding experiment A. The first three eigenvalues are approximately equal to 40.6s, 15.7s, 7.9s in the full model and are approximately equal to 49.4s, 16.6s, 7.9s, respectively, in the Holdsworth and Glynn model. The maximum deviation is also equal to 20%. Moreover, Experiment B justifies the eigenvalue *dependence on the cavity geometry* in the both considered models. The deviation for the eigenvalues due to the cavity geometry changes is about 18% (Tab. 1A)

Table 1A. *The eigenvalues difference due to the cavity geometry changes in the full model*

Eigenvalue	T_1	T_2	T_3
Experiment A	34.6	13.3	6.7
Experiment B	40.6	15.7	7.9
Deviation	17%	18%	18%

Experiment C. At the first glance in Experiment C, there are not a new specificities (in comparison with previous experiments) in the difference between the eigenvalues obtained from the considered models (Fig. 4A). Likewise, as in previous experiments, the first four eigenvalues are approximately equal to 62.8s, 20.1s, 9.75s, 5.65s in the full model and are approximately equal to 70.4s, 20.8s, 9.85s, 5.6s, respectively, in the Holdsworth and Glynn model. The maximum deviation is equal to 11%. However, more careful observation of the spectrums reveals the small peak at about 23.3s (Fig. 4A, b). The calculation at a higher temporal resolution shows the new resonant peak at 23.36s (Fig. 5A), which is not confirmed by the Holdsworth and Glynn model. Moreover, the deflections of the first mode obtained by the full model, are not in agreement with the deflections obtained by the Holdsworth and Glynn model (Fig. 6A). The first and the second (23.36s) modes of the full model reveal the staggered order for nodes/antinodes locations (Fig. 6A, a; Fig. 7A), that is not observed in the first and in others modes of the Holdsworth and Glynn model. Thus, in Experiment C the principal distinctions of the full model are that (i) the second mode doesn't coincide with any mode of the thin-plate model and (ii) the deflections of the first modes reveal different spatial distributions. Nevertheless, for coinciding (corresponding) eigenvalues the deflections in the modes are in agreement for the two considered models (Fig. 6A, b; Fig. 6A, c).

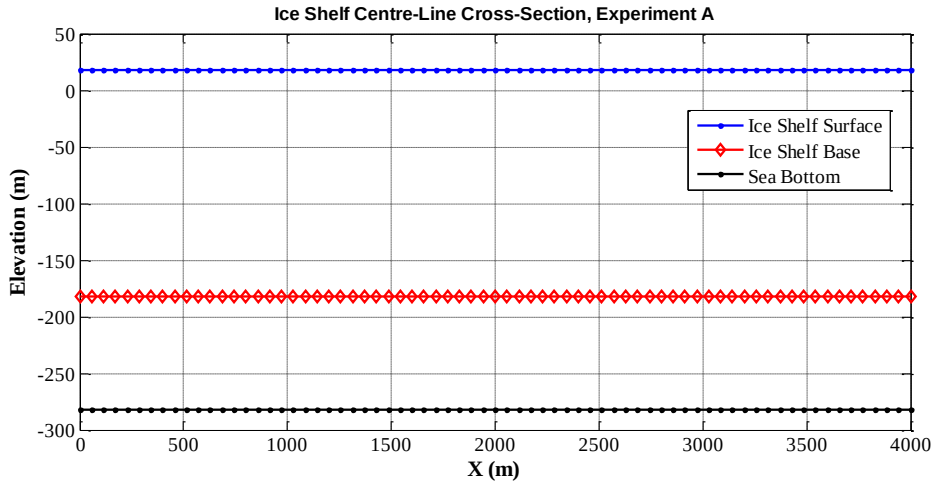

Fig. 1A, a

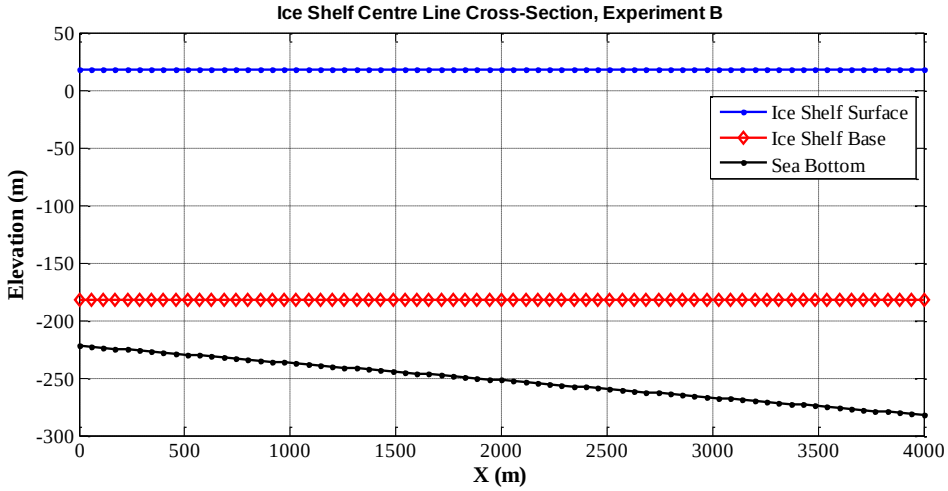

Fig. 1A, b

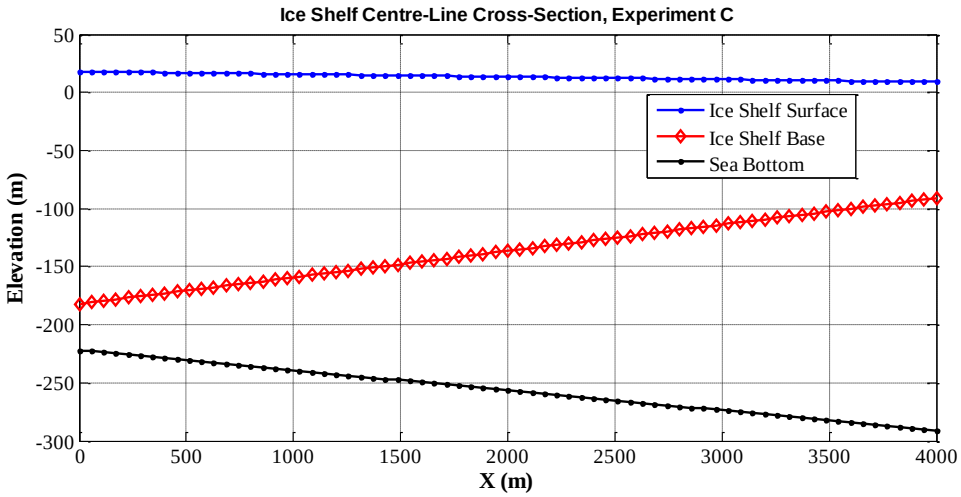

Fig. 1A, c

Figure 1A. The ice-shelf and the cavity geometries that are considered in the three numerical experiments (A, B, C).

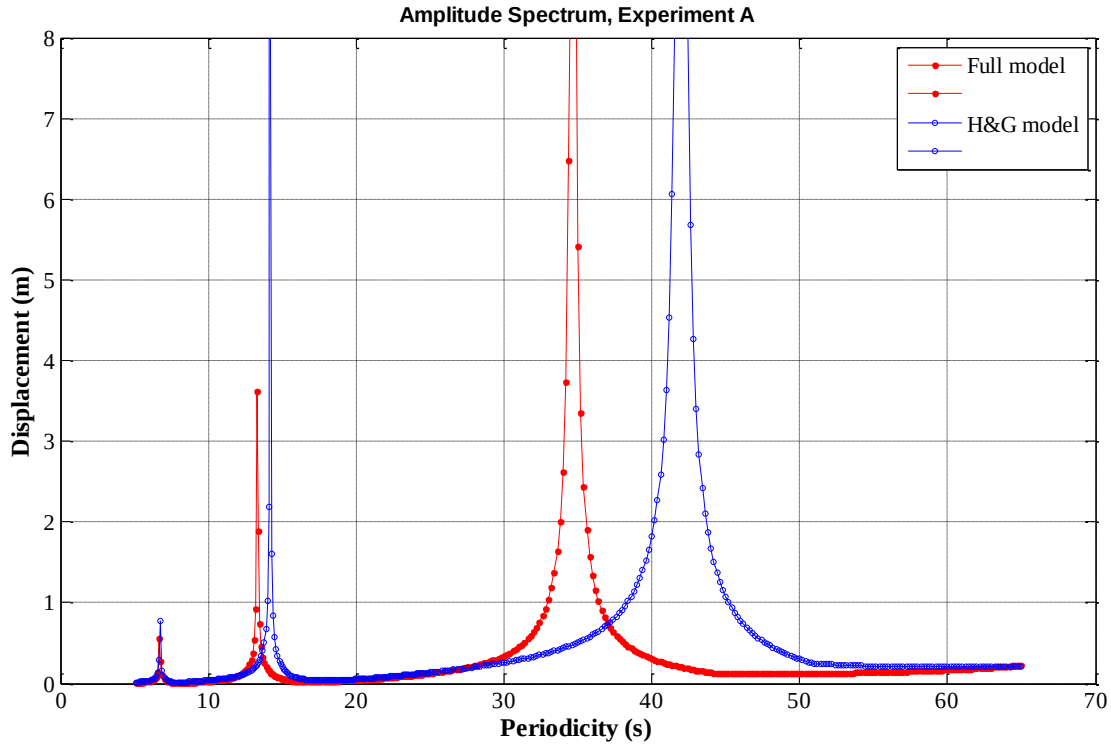

Fig. 2A, a

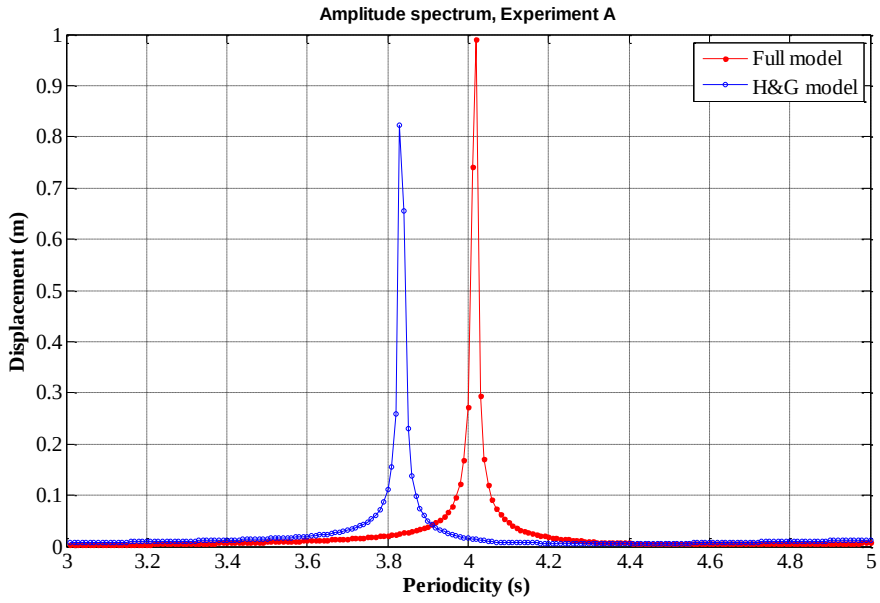

Fig. 2A, b

Figure 2A. The amplitude spectrums – maximal ice-shelf deflection versus ocean wave periodicity – obtained in Experiment A (Fig. 1A, a). The red curve is the amplitude spectrum derived from the full model. The blue curve is the amplitude spectrum obtained by the Holdsworth and Glynn model.

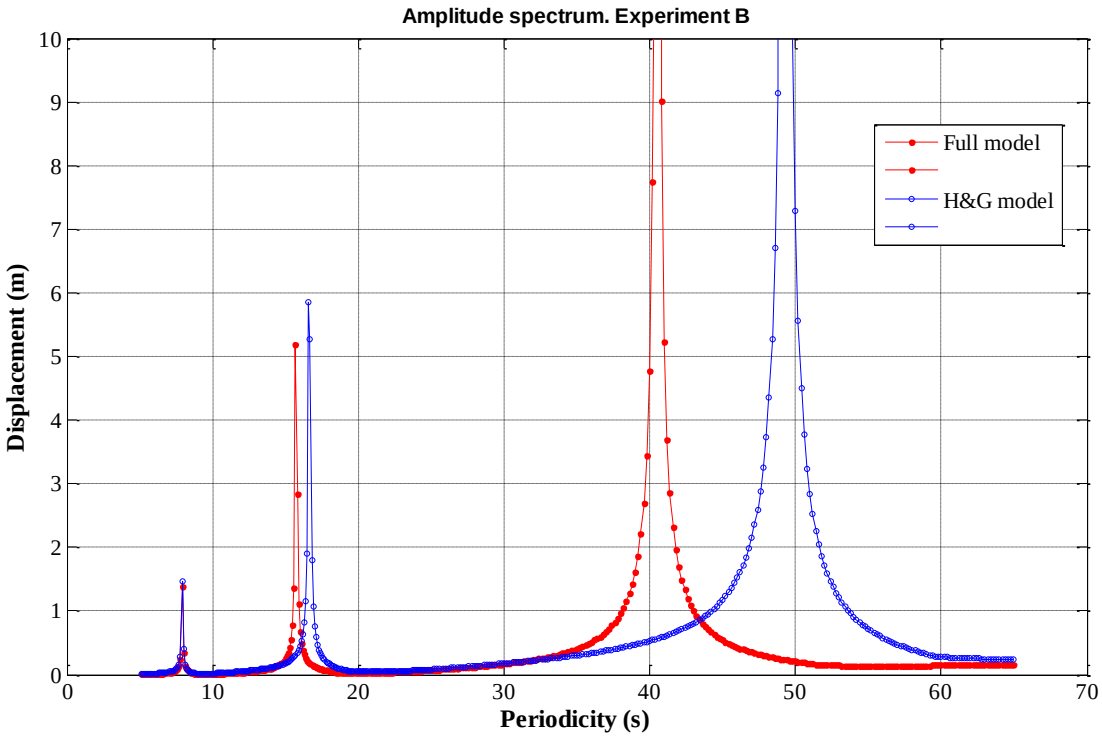

Figure 3A. The amplitude spectrums obtained in Experiment B (Fig. 1A, b). The red curve is the amplitude spectrum obtained by the full model. The blue curve is the amplitude spectrum obtained by the Holdsworth and Glynn model.

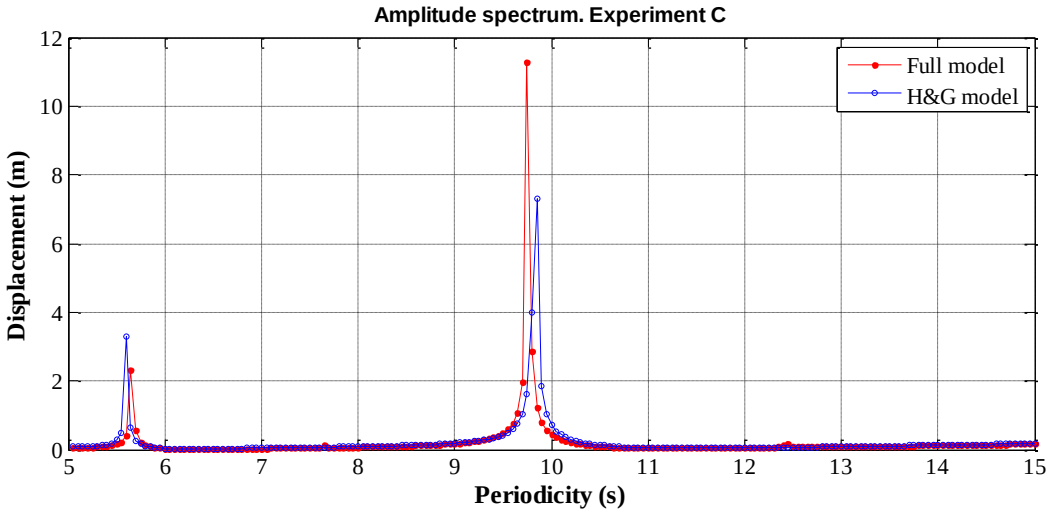

Fig. 4A, a

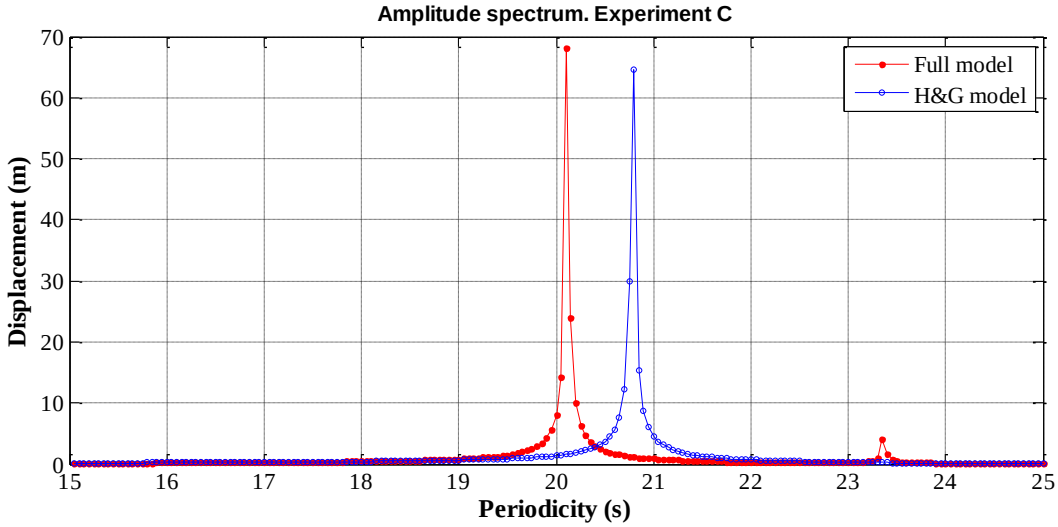

Fig. 4A, b

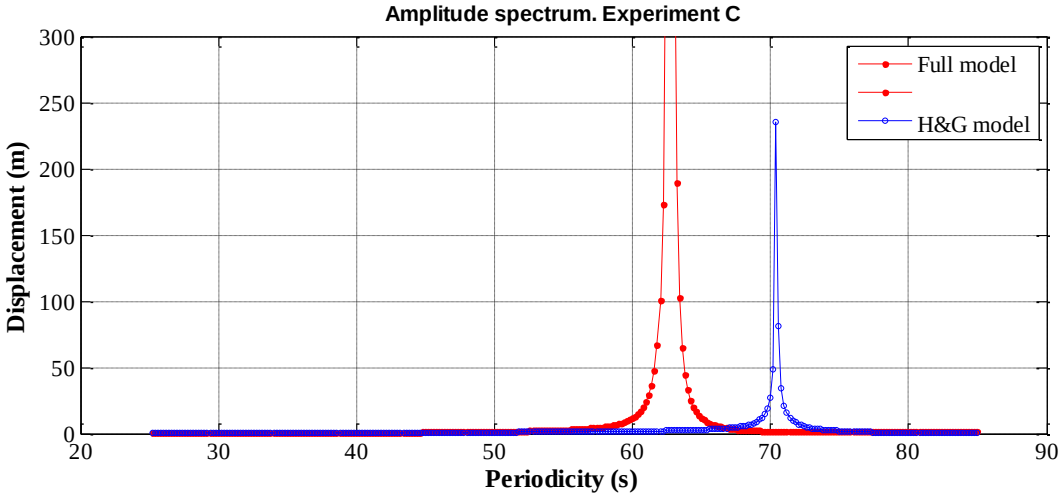

Fig. 4A, c

Figure 4A. The amplitude spectrums obtained in Experiment C (Fig. 1A, c). The red curve is the amplitude spectrum obtained by the full model. The blue curve is the amplitude spectrum obtained by the Holdsworth and Glynn model.

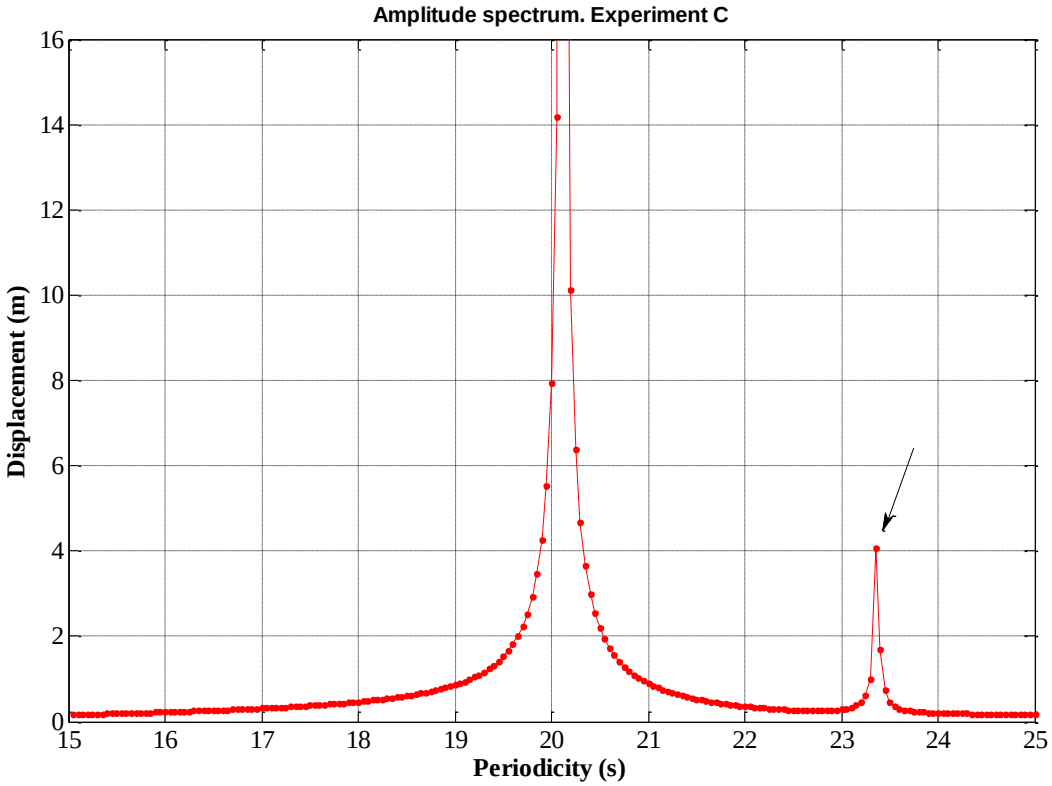

Fig. 5A, a

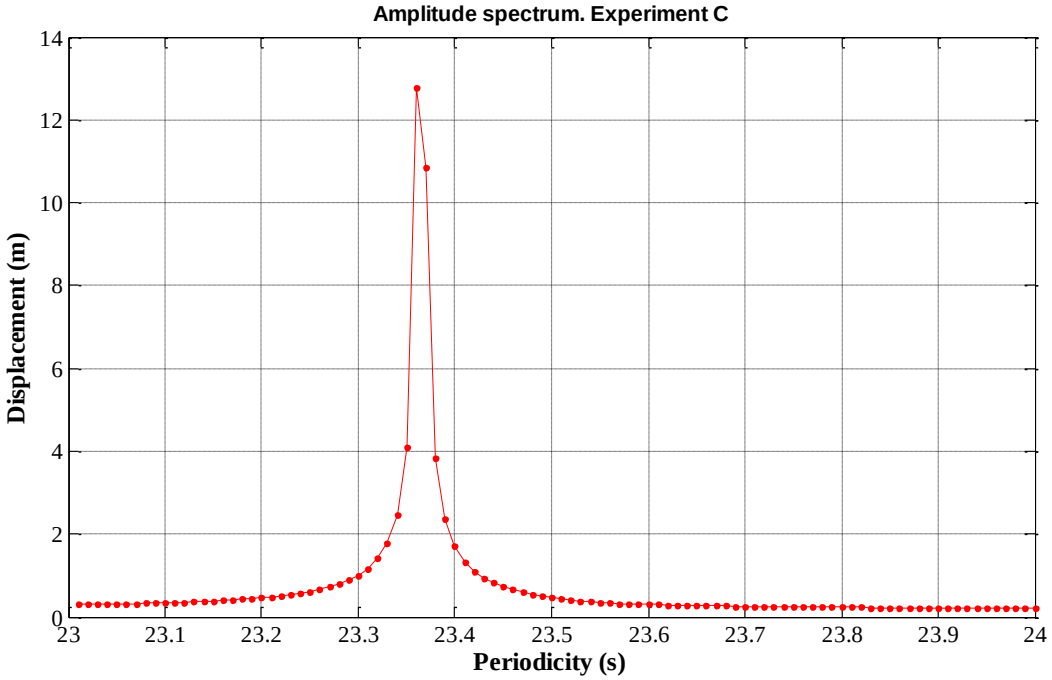

Fig. 5A, b

Figure 5A. The amplitude spectrums obtained in Experiment C (Fig. 1A, c) at different temporal resolutions: **a)** temporal resolution is equal to 0.05s; **b)** temporal resolution is equal to 0.01s.

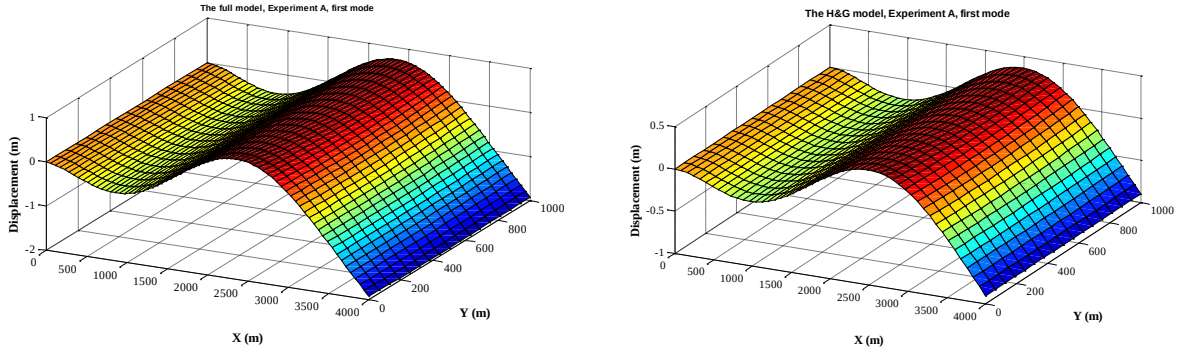

Fig. 5A, a

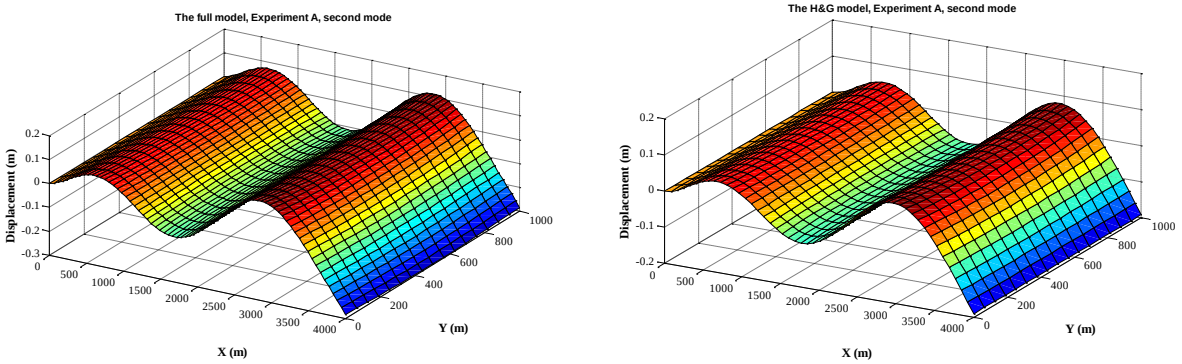

Fig. 5A, b

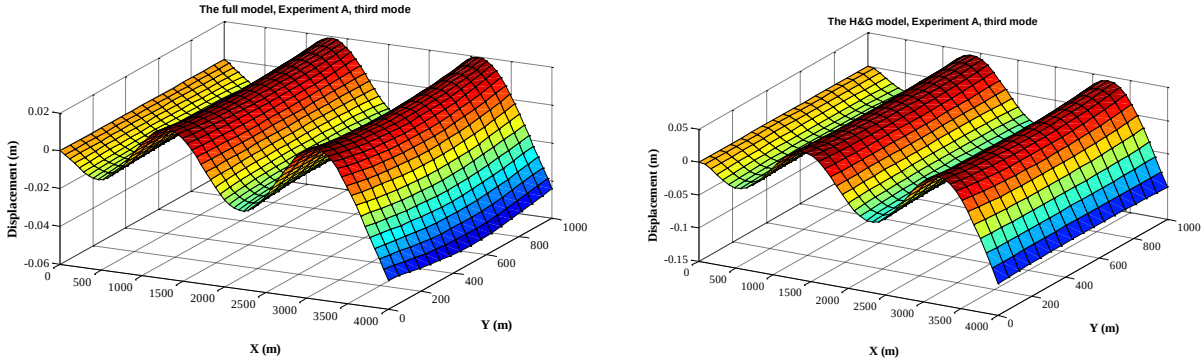

Fig 5a, c

Figure 5A. Ice-shelf deflections obtained for the first three modes in **Experiment A**. Left plots show the deflections obtained by the full model. Respectively, right plots show the deflections obtained by the Holdsworth and Glynn model. **a)** periodicities are equal to 34.2s and to 42s, respectively; **b)** periodicities are equal to 13.3s and to 14.2s, respectively; **c)** periodicities are equal to 6.7s and to 6.8s, respectively. Young's modulus $E = 9\ GPa$, Poisson's ratio $\nu = 0.33$ (Schulson, 1999), the amplitude of the incident wave is equal to 0.1m.

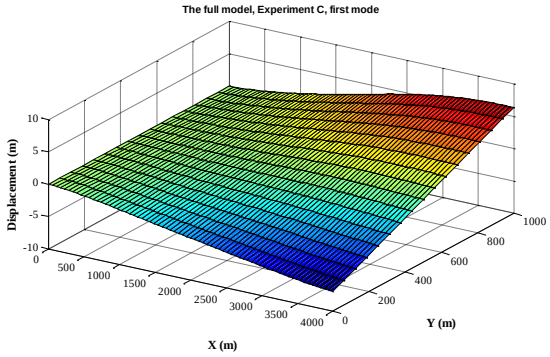

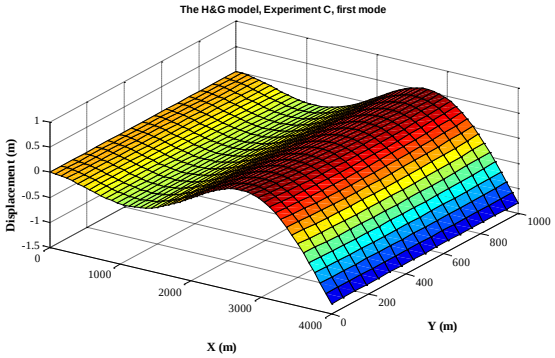

Fig. 6A, a

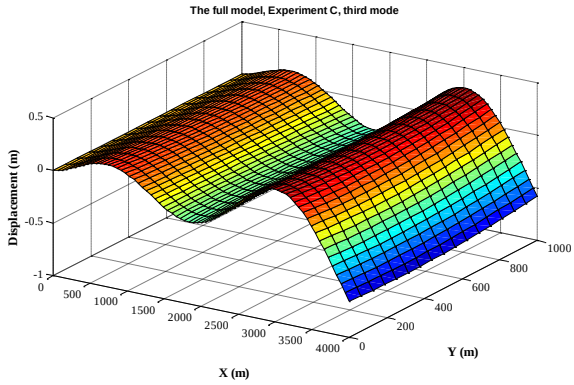

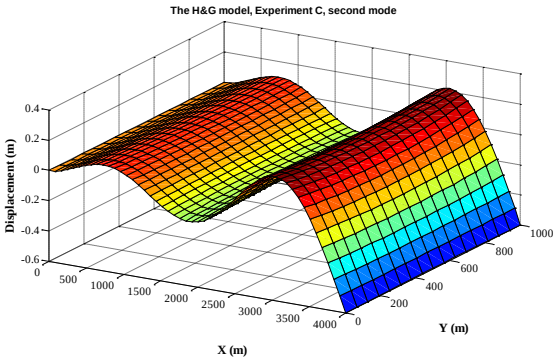

Fig. 6A, b

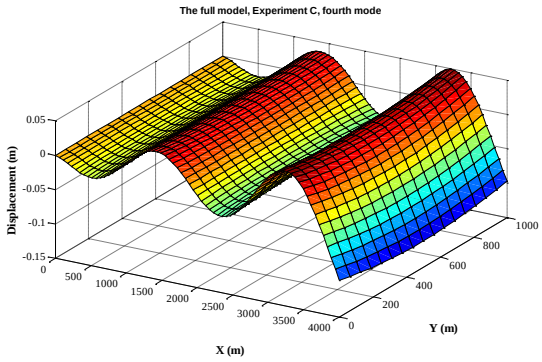

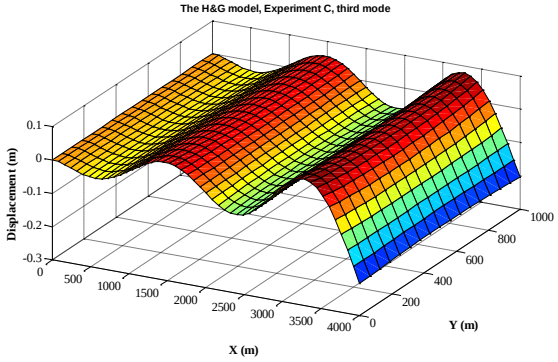

Fig. 6A, c

Figure 6A. Ice-shelf deflections obtained in Experiment C. Left plots show the deflections obtained by the full model for the first, third and fourth modes. Respectively, right plots show the deflections obtained by the Holdsworth and Glynn model for the first three modes. **a)** periodicities are equal to 34.2s and to 42s, respectively; **b)** periodicities are equal to 13.3s and to 14.2s, respectively; **c)** periodicities are equal to 6.7s and to 6.8s, respectively. Young's modulus $E = 9\ GPa$, Poisson's ratio $\nu = 0.33$ (Schulson, 1999).

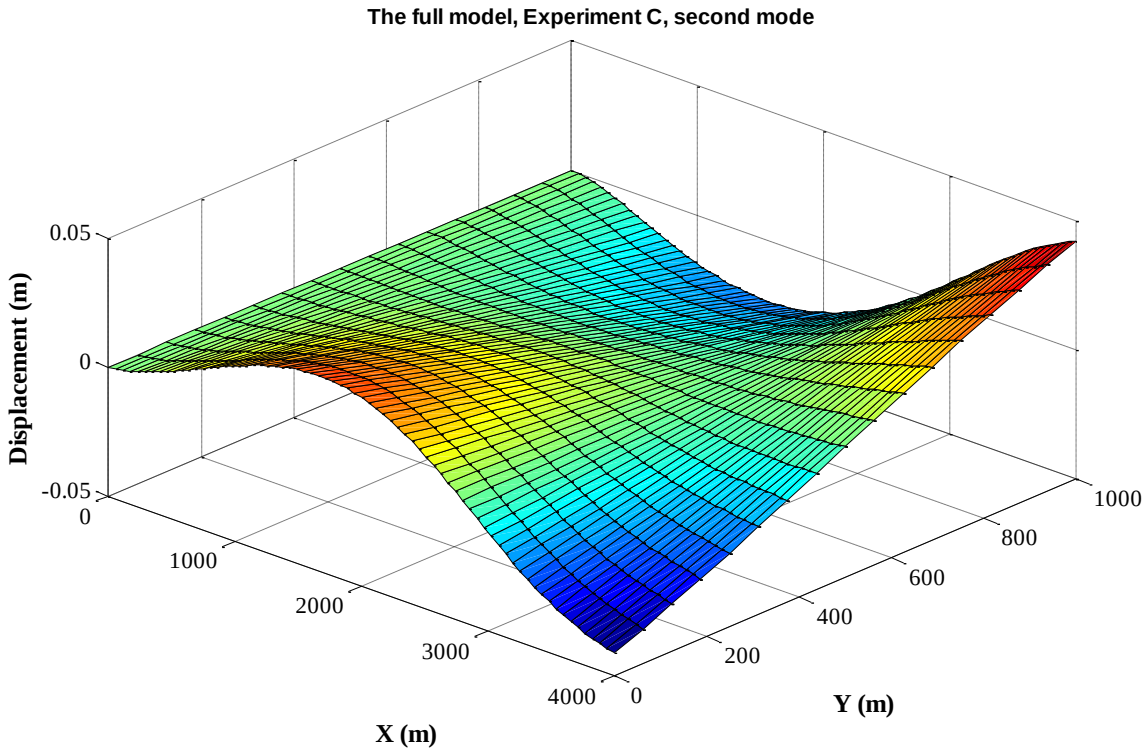

Figure 7A. Ice-shelf deflections obtained in Experiment C in the full model for the second mode (23.36s).

Stresses growing as the result of the resonant impact

The shear stress achieves the maximum beside the grounding line (Fig. 8A). For instance, in Experiment A nearly resonant forcing, which corresponds to the second eigenvalue (Fig. 2A, a), induces the threshold value ($10^6\ Pa$) in the maximum, if the amplitude of the incident wave becomes about 0.5 m. Hence, we can suppose that the long-term forcing can cause fracture of this ice-shelf, which is considered in Experiment A. Moreover, we can obtain such stress distributions for any ice-shelf geometry and for any resonant peak to estimate risks of the impact of the nearly resonant incident waves.

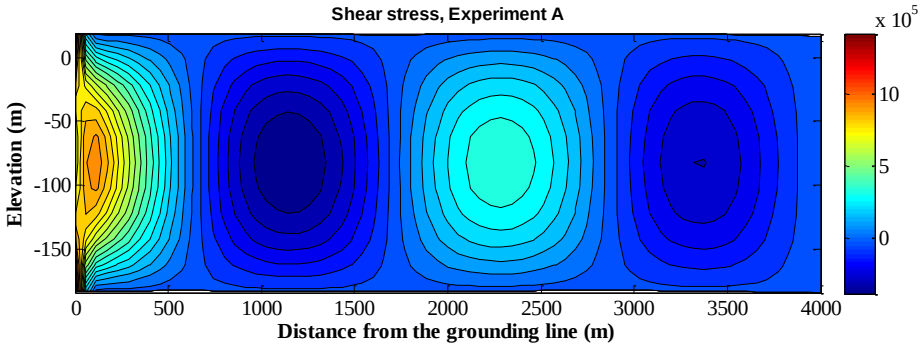

Fig. 8A, a

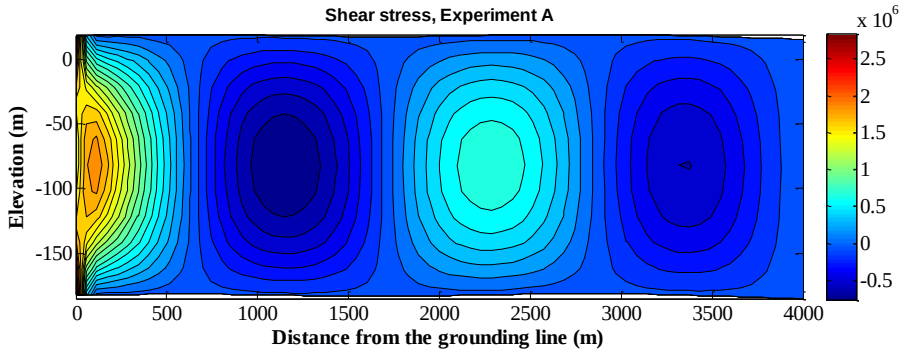

Fig. 8A, b

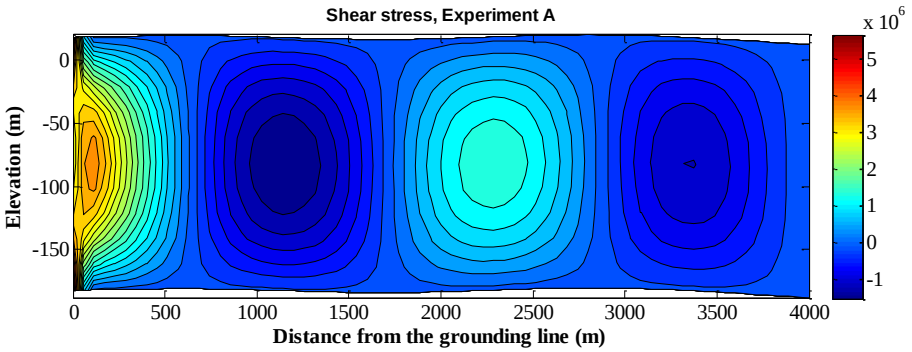

Fig. 8A, c

Figure 8A. The shear stress distribution in the vertical cross-section along the centre-line. The distributions have been obtained in Experiment A for the second mode. The incident wave amplitude is equal to **a**) 0.5 m; **b**) 1 m; **c**) 2 m.

Motivation of the manuscript

Thus, relying on the referees' comments, the motivation of the manuscript is the following. First, to introduce the method, which provides the stability of the numerical solution in the full model, which implies the coupling of the fundamental momentum equations with the wave equation for the water layer. Second, to compare the results obtained by the two models with intent to reveal the principal distinctions, if they exist, and specifics of the full model. (I don't maintain the opinion that the full model provides more correct results and I agree that the verification of the model against observations/measurements is needed to encourage the choice of the full model).

I agree to improve English in the manuscript using the help of the professional editors of Copernicus Publisher.

Thanks and all the best,

Yuri V. K.